Tetrahedral Distortion and Thermoelectric Performance of the Ag-Substituted $CuInTe_2$ Chalcopyrite Compound

Chenyang Wang,[†] *Quanying Ma,*[†] *Huarui Xue,*[†] *Qin Wang,*[†] *Pengfei Luo,*[†] *Jiong Yang,*[‡] *Wenqing Zhang,*[§] *Jun Luo,*[*,†]

†School of Materials Science and Engineering, Shanghai University, 99 Shangda Road, Shanghai 200444, China

‡Materials Genome Institute, Shanghai University, 99 Shangda Road, Shanghai 200444, China

§ Department of Physics, Shenzhen Institute for Quantum Science and Engineering, and Guangdong Provincial Key-Lab for Computational Science and Materials Design, Southern University of Science and Technology, Shenzhen 518055, China

*Corresponding Authors. E-mail: junluo@shu.edu.cn (J.L.).

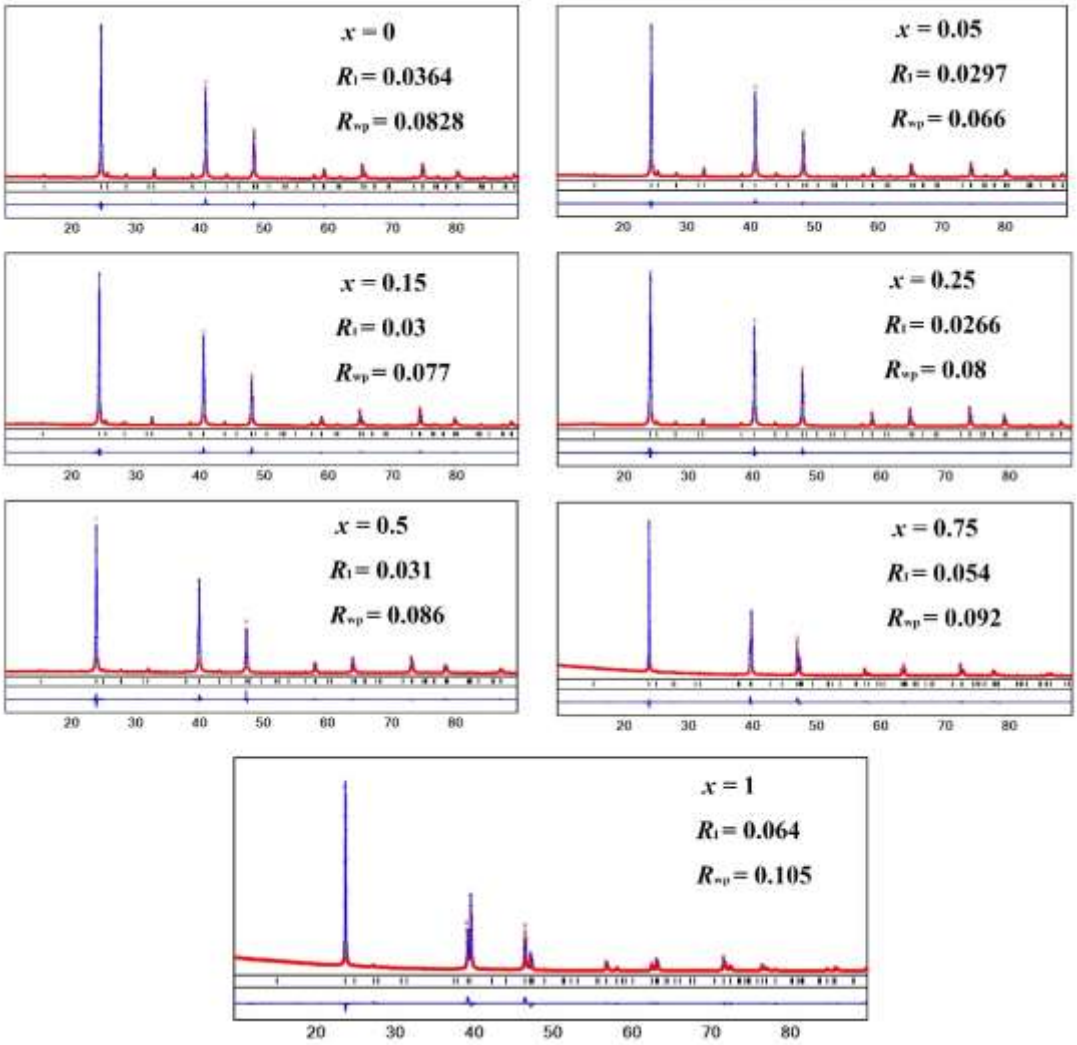

Figure S1. XRD diffraction data including profile fit, profile difference and profile residuals of the corresponding Rietveld refinement for $Cu_{1-x}Ag_xInTe_2$ (x = 0–1) samples.

Table S1 Atomic coordinates for $Cu_{1-x}Ag_xInTe_2$ (x = 0–1) samples

Composition	4a (1/2, 0, 3/4)	4b (0, 0, 1/2)	8d (1/4, y, 3/8)
$CuInTe_2$	Cu	In	Te, y = 0.27743(10)
$Cu_{0.95}Ag_{0.05}InTe_2$	Cu, Ag	In	Te, y = 0.27667(8)
$Cu_{0.85}Ag_{0.15}InTe_2$	Cu, Ag	In	Te, y = 0.2750(1)
$Cu_{0.75}Ag_{0.25}InTe_2$	Cu, Ag	In	Te, y = 0.2735(1)
$Cu_{0.5}Ag_{0.5}InTe_2$	Cu, Ag	In	Te, y = 0.2673(2)
$Cu_{0.25}Ag_{0.75}InTe_2$	Cu, Ag	In	Te, y = 0.2569(4)
$AgInTe_2$	Ag	In	Te, y = 0.2499(12)

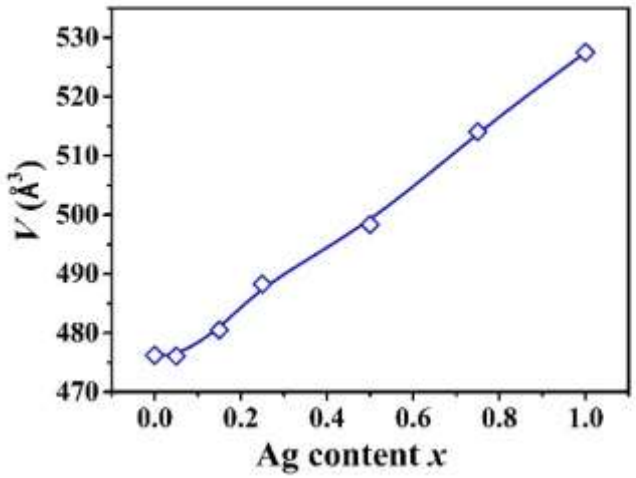

Figure S2. Compositional dependence of cell volume for $Cu_{1-x}Ag_xInTe_2$ (x = 0–1) samples.

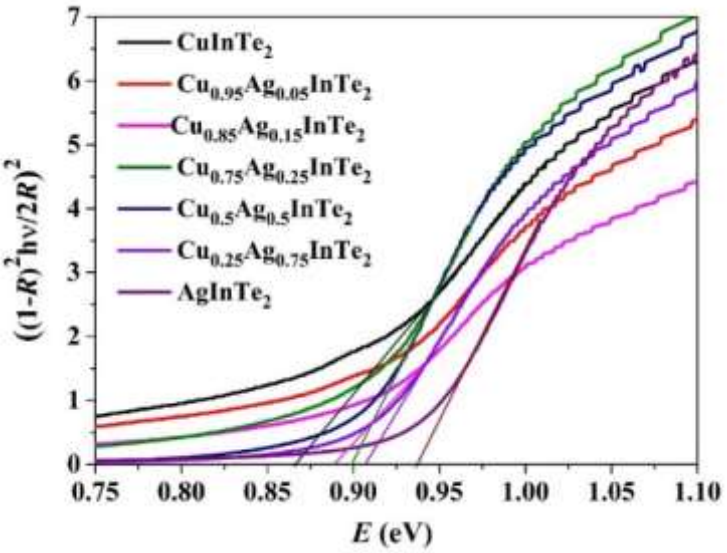

Figure S3. Photon energy dependence of $((1-R)^2h\nu/2R)^2$ for the $Cu_{1-x}Ag_xInTe_2$ (x = 0–1) samples.

The band gap can be estimated by the extrapolation of the linear fitting.

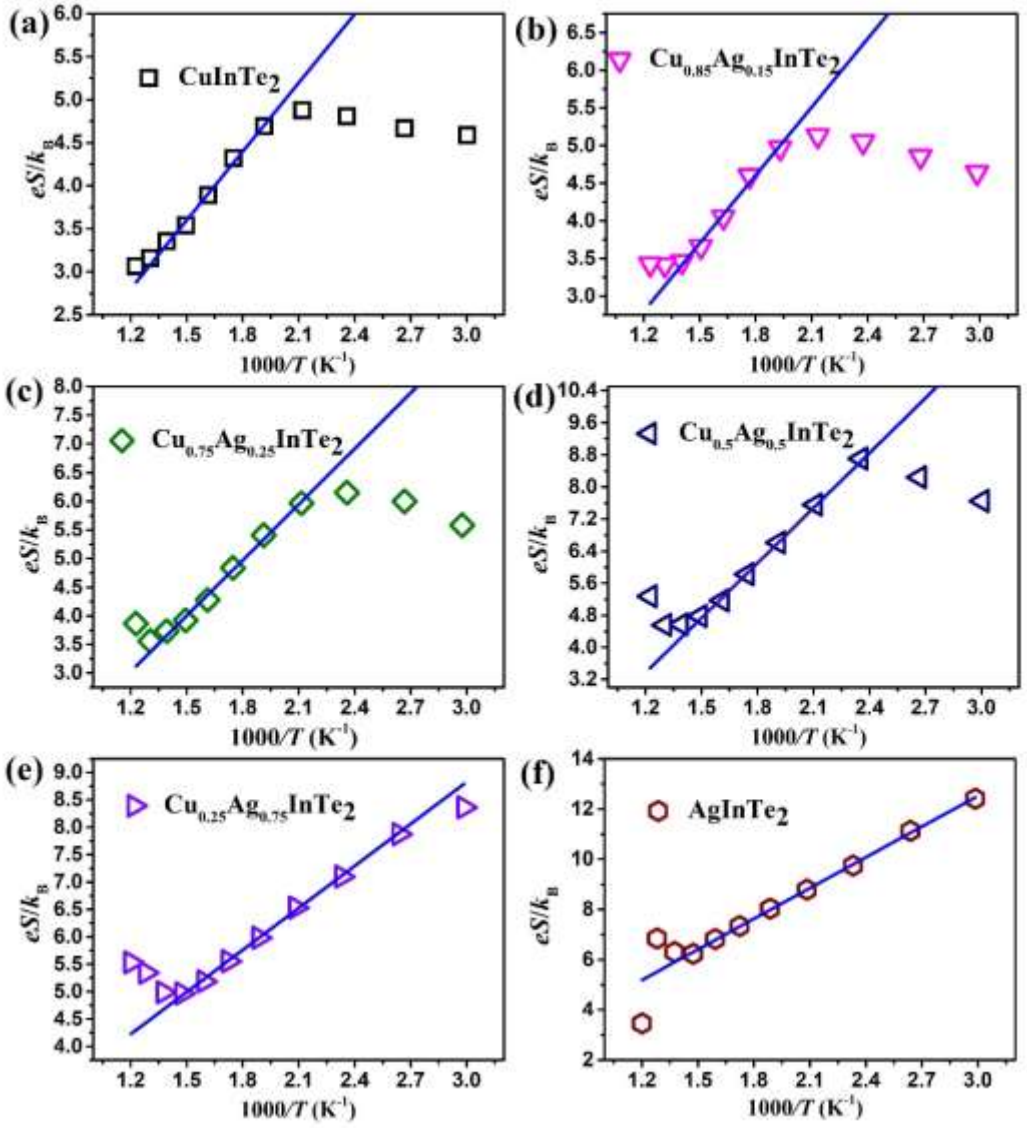

Figure S4. (eS/k_B) vs 1000/T plots and linear fitting for $Cu_{1-x}Ag_xInTe_2$ (x = 0–1) samples.

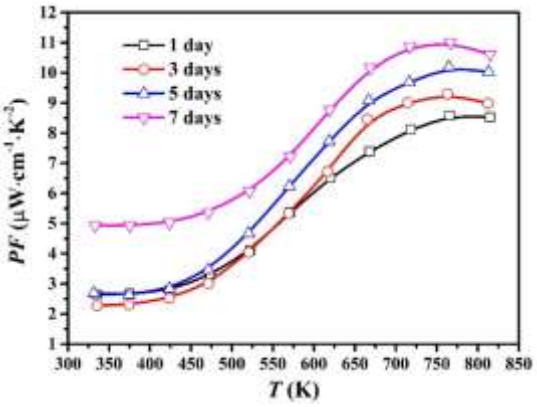

Figure S5. Temperature-dependent power factors for $CuInTe_2$ samples annealed at 923 K for 1

day, 3 days, 5 days and 7 days, respectively.

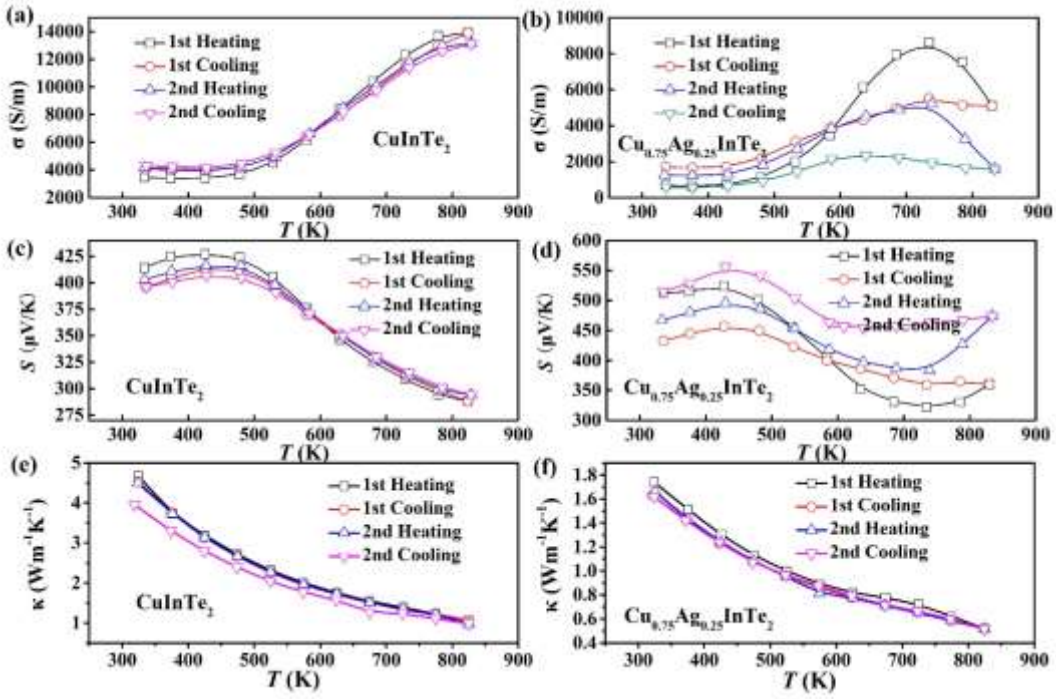

Figure S6. Repeatedly measured temperature dependent electrical conductivities, Seebeck coefficients and thermal conductivities for $CuInTe_2$ and $Cu_{0.75}Ag_{0.25}InTe_2$.

As shown in Figure S6a, c and e, some slight changes in electronic and thermal transport are observed for the $CuInTe_2$ sample. While for $Cu_{0.75}Ag_{0.25}InTe_2$ sample, its thermal conductivity exhibits some small changes, but its electronic transport properties show obvious changes in the heating-cooling processes. It seems like that the thermal stability became worse after Ag doping. We suspect these changes in thermal properties of $Cu_{1-x}Ag_xInTe_2$ samples may is related to the defects existing in the samples, since the defects have a big effect on the thermoelectric properties of diamond-like semiconductors. The origin of these changes needs more experiments and characterizations. This problem will be analyzed and resolved in our future work.

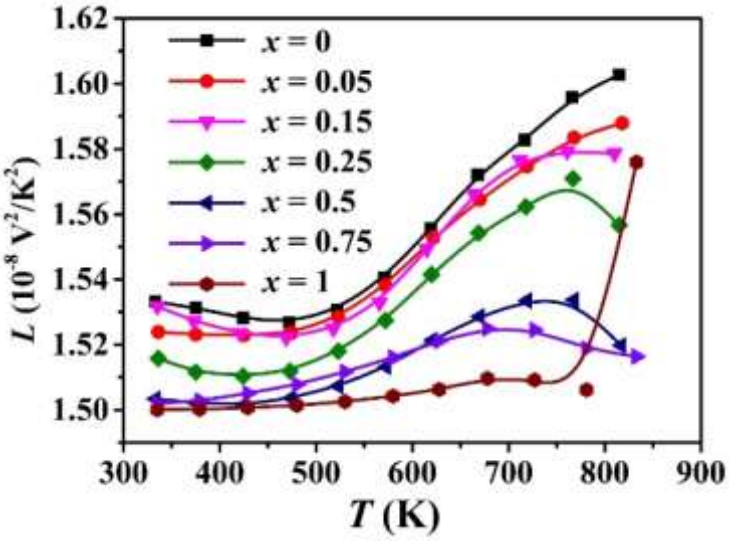

Figure S7. Temperature-dependent Lorenz number for $Cu_{1-x}Ag_xInTe_2$ (x = 0–1) samples.

Table S2 Calculated intrinsic carrier mobility and experimental mobility data for $CuInTe_2$ and $Cu_{0.75}Ag_{0.25}InTe_2$ at room temperature

Sample	B (GPa)	m_b^*	μ_0 ($cm^2V^{-1}s^{-1}$)	μ_{exp} ($cm^2V^{-1}s^{-1}$)
$CuInTe_2$	46	0.472 m_e	36	31
$Cu_{0.75}Ag_{0.25}InTe_2$	41.7	0.504 m_e	27	28

The intrinsic carrier mobility was calculated according to the equation $\mu_0 = A_0 B^S (m_b^*)^{-t}$, the bulk modulus B and band effective mass m_b^* are required, which can be derived from the DFT calculations.[1] As can be seen, the values of μ_0 are close to those of μ_{exp} for two samples. Furthermore, the mobility of undoped $CuInTe_2$ is slightly higher than that of Ag-doped $Cu_{0.75}Ag_{0.25}InTe_2$ at RT. However, the difference in μ_0 between two samples is much larger than that in μ_{exp} because of the effect of the carrier concentration. In addition, after Ag doping, the contribution of ionization scattering should be considered for scattering mechanism, which is likely

one of the reasons for the increased mobility of intermediate alloys. The similar phenomenon (μ increases after doping) is also observed in other systems (e.g. $CuIn_{1-x}Zn_xTe_2$,[2] $Cu_{1-x}InZn_xTe_2$,[2] $In_{0.98}Cd_{0.02}Te$[3]).

Table S3 Parameters used for the modeling in this work

Symbol	Representation	Value	Reference
V	Volume per atom	29.72 Å^3/atom (x = 0); 29.84 Å^3/atom (x = 0.05); 30.16 Å^3/atom (x = 0.15); 30.34 Å^3/atom (x = 0.25); 31.10 Å^3/atom (x = 0.5); 31.73 Å^3/atom (x = 0.75); 32.58 Å^3/atom (x = 1).	
θ_D	Debye temperature	246 K (for x = 0, 0.05, 0.15); 234 K (for x = 0.25); 229 K (for x = 0.5); 225 K (for x = 0.75); 220 K (for x = 1);	4
γ	Grüneisen parameter	1.86	5
v	Average sound velocity	2176.65 m·s^{-1} (for x = 0, 0.05, 0.15); 1893.84 m·s^{-1} (for x = 0.25); 1800.18 m·s^{-1} (for x = 0.5); 1974.45 m·s^{-1} (for x = 0.75); 1962.18 m·s^{-1} (for x = 1)	4
h	Plank constant	6.62607015×10^{-34} J·s	
v_p	Poisson ratio	0.299 (for x = 0, 0.05, 0.15); 0.315 (for x = 0.25); 0.324 (for x = 0.5); 0.320 (for x = 0.75); 0.318 (for x = 1)	4
W	$\Delta_{bulk\ modulus}/\Delta_{strain}$	3	6

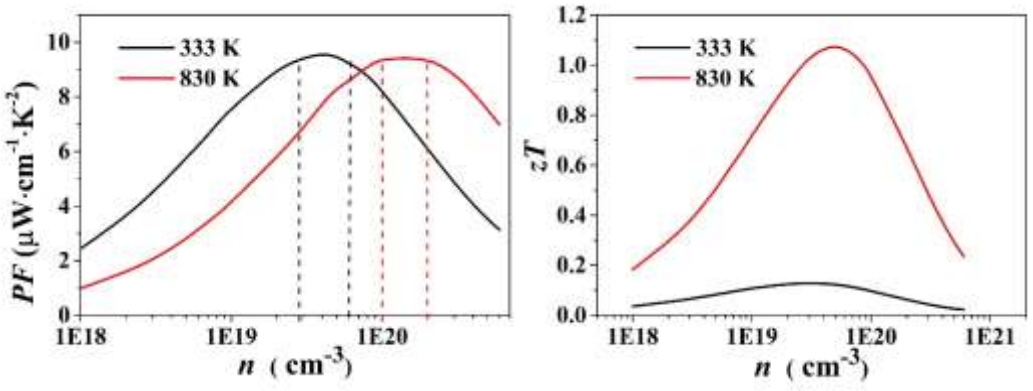

Figure S8. Calculated power factors and figure of merit *zT* values versus carrier concentration in $CuInTe_2$ at 333 K and 830 K.

For the calculations in Figure S8, the parameters of density of states effective mass $m^* = 1.0\ m_0$, deformation potential constant $E_{def} = 7$ eV and elastic constant for longitudinal vibrations $C_l = 7.062 \times 10^{10}$ Pa are used. The details of calculation method can be found in the literature.[7] Based on the obtained average lattice thermal conductivities of $Cu_{1-x}Ag_xInTe_2$ samples, the calculated maximum *zT* values are around 0.128 at 333 K and 1.076 at 830 K. The actual maximum zT value is already above the predicted value, which is not rare in the reports for $CuInTe_2$-based materials, since some assumptions differ from the actual situations.

References

1. Yan, J.; Gorai, P.; Ortiz, B.; Miller, S.; Barnett, S. A.; Mason, T.; Stevanovic, V.; Toberer, E. S., Material descriptors for predicting thermoelectric performance. *Energy Environ. Sci.* **2015,** *8* (3), 983-994.

2. Yang, J.; Chen, S.; Du, Z.; Liu, X.; Cui, J., Lattice defects and thermoelectric properties: the case of p-type $CuInTe_2$ chalcopyrite on introduction of zinc. *Dalton Trans.* **2014,** 43 (40), 15228-15236.

3. Pan, S.; Liu, H.; Li, Z.; You, L.; Dai, S.; Yang, J.; Guo, K.; Luo, J., Enhancement of the thermoelectric performance of InTe via introducing Cd dopant and regulating the annealing time. *J. Alloys Compd.* **2020,** 813, 152210.

4. Zhong, Y.; Wang, P.; Mei, H.; Jia, Z.; Cheng, N. Elastic, vibration and thermodynamic properties of $Cu_{1-x}Ag_xInTe_2$ (x = 0, 0.25, 0.5, 0.75 and 1) chalcopyrite compounds via first principles, *Semicond. Sci. Tech.* **2018**, 33, 065014.

5. Sharma, S.; Verma, A.S.; Bhandari, R.; Jindal, V.K. Ab initio studies of structural, elastic and thermal properties of copper indium dichalcogenides ($CuInX_2$: X=S, Se, Te), *Comp. Mater. Sci.* **2014**, 86, 108-117.

6. Wang, H.; Wang, J.; Cao, X.; Snyder, G.J. Thermoelectric alloys between PbSe and PbS with effective thermal conductivity reduction and high figure of merit, *J. Mater. Chem. A* **2014**, 2 3169-3174.

7. Shen, J.; Chen, Z.; Lin, S.; Zheng, L.; Li, W.; Pei, Y. Single parabolic band behavior in thermoelectric p-type $CuGaTe_2$, *J. Mater. Chem. C*, **2016**, 4, 209-214.